Evolution of electron temperature and electron density in indirectly driven spherical implosions

N. C. Woolsey,* B. A. Hammel, C. J. Keane, A. Asfaw, C. A. Back, J. C. Moreno, and J. K. Nash
University of California, Lawrence Livermore National Laboratory, P.O. Box 808, Livermore, California 94551

A. Calisti, C. Mossé, R. Stamm, and B. Talin
URA 773 case 232, Université de Provence, Centre St. Jérôme, 13397 Marseille Cedex 20, France

L. Klein
Department of Physics, Howard University, Washington, DC 20059

R. W. Lee
Department of Physics, 366 LeConte Hall–7300, University of California, Berkeley, California 94720
(Received 29 July 1996; revised manuscript received 4 February 1997)

Using spectroscopic measurements to extract electron density and temperature, we construct simulation-independent time histories of the assembly and disassembly phase of an imploding core. To achieve this, we show the hot dense plasma produced by indirectly imploding a gas-filled microsphere is a reproducible and reliable plasma source. We further show that this plasma is suitable for detailed hydrodynamic and spectroscopic studies, and that the plasma provides a useful testbed for nonlocal thermodynamic equilibrium plasma studies at extreme conditions. [S1063-651X(97)09908-X]

PACS number(s): 52.70.La, 52.25.Nr, 52.50.Lp, 52.58.Ns

The study of hot density plasmas is of interest to those studying stellar atmospheres, inertial confinement fusion plasmas, strongly coupled plasmas, and radiative properties at extreme conditions [1]. The production and diagnosis of such plasmas is made difficult by their inherently transient nature, their small spatial extent, and the need to verify that the plasmas are hydrodynamically stable and reproducible. Here we present the spectroscopic results from a hydrodynamically stable reproducible high-energy density plasma, and use it to track the implosion dynamics in a manner that is *independent* of hydrodynamic simulation. The plasma produced is contained within an implosion core of a plastic microsphere prepared to have a small amount of seed gas that is used as a probe of the hot dense matter. Although there have been previous reports of single, peak high-density results from implosion cores, the emission is dominated in those plasmas by effects of nonsphericity of the implosions, hydrodynamics instabilities, laser nonuniformities, or laser-plasma instabilities. The results reported here are derived from the first stable and reproducible hot dense plasmas, and therefore can be used to address questions on both the formation of these plasmas and the effects of the extreme conditions on ions embedded in them.

In these plasmas, where extreme conditions such as 1×10^{24} cm^{-3} and 1000 eV can be reached, a medium-Z dopant, in the present case Ar, is introduced in trace amounts into the low Z, i.e., D_2, gas-filled core contained in a spherical shell of CH plastic [2,3]. The dopant concentration is made small enough to minimize any perturbation, due to radiative cooling, of the hydrodynamics of the target, while keeping the concentration high enough to produce observable x-ray emission. Further, since spectral line shapes are the primary diagnostic, it is essential to maintain optically thin spectral lines; with these considerations the concentration of the Ar dopant is controlled to ensure that the K-shell 1–3 transitions, centered at 3.365 and 3.150 Å, respectively [4], have optical depths of 0.2–0.4. In the following we use the detailed Stark broadening calculations of the complete profile, i.e., the Ar XVII $1s^2\ ^1S-1s3p\ ^1P$ (Heβ) [2,3], together with the Li-like $2l3l'$ and $3l3l'$ satellites to the Heβ transition, to determine the temperature and density history of the implosion core [2,5]. The experimental parameters are fixed to drive the microsphere implosion to radial compression ratios of $\sim$6, which allows us to map the sphericity of the implosion by x-ray imaging, and limits the growth of hydrodynamic instabilities that occur at high aspect ratios.

To provide the diagnostic information a N_e-T_e grid of theoretical line profiles including the dielectronic satellites was generated using TOTAL-II [6]; these profiles are convolved with the instrument response, and compared directly to the experimental data. Efficient fitting of experimental data with the predicted line shapes is ensured by interpolating across the N_e-T_e grid [7]. The shape of the Heβ transition, ignoring the Li-like satellites, determines the N_e, while fitting the satellites *and* the Heβ line determines the T_e. Fitting the Li-like satellites on the low-energy side of Heβ line is an accurate T_e diagnostic below 800 eV.

The implosions are indirectly driven using a soft-x-ray radiation source created with NOVA [8]. Five beams, symmetrically arranged, enter each end of a 1.6-mm-diameter, 2.55-mm-long gold cylinder, the hohlraum target, through 0.8-mm-diameter entrance holes. Each beam has a temporally square 1-ns pulse shape and 2 kJ of energy at a wavelength of 0.353 μm. The beams strike the interior wall creating a plasma that radiates efficiently at soft-x-ray energies.

*Present address: School of Mathematics and Physics, Queen's University of Belfast, Belfast BT7 1NN, Northern Ireland. Electronic address: n.woolsey@qub.ac.uk

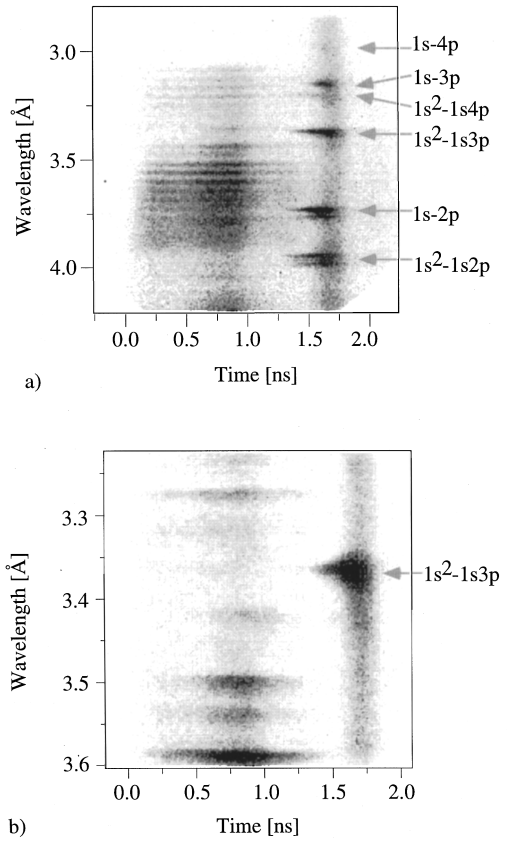

FIG. 1. Spectroscopic data recorded using the (a) survey spectrometer, and (b) high-resolution spectrometer after correction. The Ar K-shell features are labeled.

The radiation field impinges on the microsphere, ablatively imploding it. The microsphere consists of a 2-μm-thick, 440-μm-diameter polystyrene shell. The polystyrene is overcoated with an impermeable 3-μm polyvinyl alcohol layer and then a 56-μm-thick CH ablator. The thickness of the CH ablator ensures that the ablation front and radiation field are excluded from the core. The gas fill is 50 atm of D_2 and 0.1 atm of Ar.

The main diagnostics are two x-ray crystal streaked spectrometers. A lower-resolution instrument ($E/\Delta E \sim 500$) uses a flat rubidium acid phthalate (RAP) crystal to cover 2.8–4.2 Å, with 25-ps temporal resolution. The higher-resolution spectrometer ($E/\Delta E \sim 1800$) uses a flat pentaerythritol (PET) crystal for detailed Heβ line-shape measurements [9]. Further, the microsphere is imaged along and perpendicular to the cylinder axis, with two gated x-ray pinhole cameras, filtered to record x-ray emission >3 keV [10].

The data were recorded on Kodak TMX-3200 film, digitized using a microdensitometer, and then corrected for film response, camera-induced distortions, filter, crystal, photocathode response, and spectrometer artifacts. The spectrometer dispersion is determined from the experimental geometry and published wavelengths for the Ar K-shell and Au M-band lines [4].

Images from the survey and the high-resolution spectrometers are shown in Fig. 1, where time increases to the right, and $t=0$ denotes the time at which the laser enters the hohlraum target. Au M-band emission is clearly seen during the 1-ns laser pulse, decaying away after the laser pulse and before the Ar K-shell emission is observed. The optically thin Heβ transition is used to diagnose the core. All spectra are spatially integrated over the core.

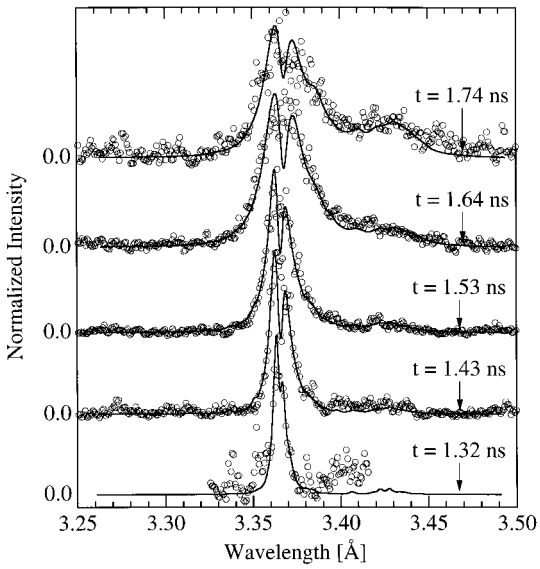

FIG. 2. Detailed measurements of the Ar Heβ transition (circles) compared to calculations of Heβ and Li-like $2l3l'$ and $3l3l'$ satellites (solid lines) for five times during the implosion.

The analysis of the data in Fig. 1 is performed by taking successive cross sections in the spectral direction through the Ar emission, and fitting the Heβ line at each time. The results are shown in Fig. 2, where the intensity versus wavelength at five times is represented. In addition, in Fig. 2, at each time we show the theoretical line profile, the Heβ transition and the associated Li-like satellites are included in the calculations. From these spectra, N_e and T_e are obtained. These fits show excellent agreement with theory so that the results of the analysis can be used to develop a time history for the implosion.

In Figs. 3(a) and 3(b) we show the N_e and T_e time histo-

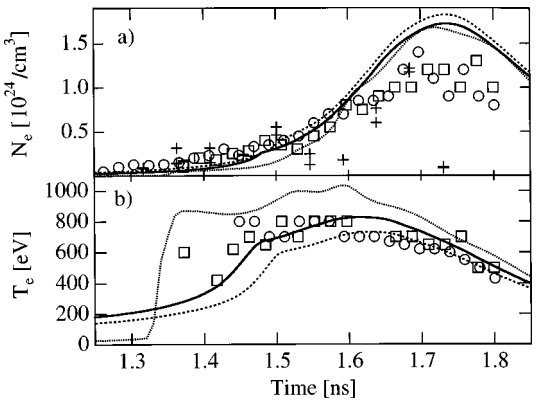

FIG. 3. Evolution of (a) N_e and (b) T_e extracted from the Ar Heβ transition shown in Fig. 1. Analysis of the high-resolution spectra (circles) and survey Heβ line (squares) are shown. Experimental histories are compared to gated x-ray imager data (crosses) and to N_e and T_e simulations of the central region (dotted line), mid-mass region (solid line), and outer region (dashed line) of the core.

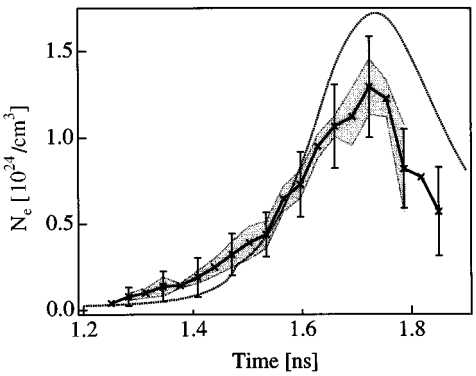

FIG. 4. N_e time histories from five similar implosions represented by the solid line. The shaded region is the rms experiment-to-experiment variation, and error bars the estimated accuracy. The dotted line is the simulated N_e.

ries derived from the analysis. The density histories in Fig. 3(a) show that the results from both high- and low-resolution spectrometers agree. The simultaneous observation of the Lyman transitions yields a bound on the ion stage distribution confirming that the optical depth of Heβ is small. Moreover, these high densities result in a steady-state evolution of N_e and T_e, so that the spectrum at each time is indicative of the local conditions. The massive shell of an imploding microsphere limits the core pressure gradients, so that the imploded core becomes a potential source for further detailed spectroscopic and hydrodynamic studies. The maximum density achieved is $\sim 1\times 10^{24}$ cm^{-3}, and the density history has a full width at half maximum of 200 ps. In Fig. 3(b) the temperature history is shown to peak at 800 eV, which is the upper bound on the T_e diagnostic.

To validate the above mapping of the time-dependent spectrum to core N_e and T_e via the detailed line profile, we need to show that the results are reproducible and reliable. To illustrate the reproducibility and consistency of these experiments, a series of five experiments under near-identical conditions were made. In each case the laser energy was 19 ± 2 kJ, and a $4\pm 2\times 10^8$ D-D neutron yield was achieved for each implosion. Using the spectral analysis techniques described, time histories for N_e from the five shots were extracted and are shown in Fig. 4. The time histories compare well, with the solid line representing the mean density and the shaded region the rms deviation, showing the small experiment-to-experiment variation.

To demonstrate the reliability of the measurement, we make recourse to the other diagnostics. First, from the x-ray imagers N_e can be determined by assuming that the fill gas is ionized, and that the image represents the core diameter. The results of this analysis are shown in Fig. 3(a) by the crosses. The latter assumption breaks down when the plastic shell assembles at ~ 1.7 ns, giving a bright continuum emission as seen in Fig. 1. Further corroboration is provided by the secondary neutron production [11], which gives a ρR of ~ 6 mg/cm^2, leading to N_e estimates of 7×10^{23} cm^{-3} in agreement with the spectroscopically determined N_e at peak T_e.

This shows these implosions to be reliable and reproducible, so that the time histories and detailed spectra can be compared to hydrodynamic simulations and detailed line-shape calculations. We show a comparison with hydrodynamic simulation in Figs. 3(a) and 3(b) between the experimental results, and a HYADES one-dimensional radiation-hydrodynamic simulation [12]. We see that there is broad agreement between experimental and simulated time histories. In the HYADES simulations the shell and core of the microsphere are modeled using an ideal gas equation of state and nonlocal thermodynamic equilibrium average-atom atomic physics. The implosion is driven with a single-temperature radiation temperature (T_r) source and multigroup radiation transport.

We note that the simulations do predict small N_e and T_e spatial gradients. The simulations, at times close to peak compression, indicate the core is near isobaric with a T_e peak at the core center. As the spectroscopic measurements presented here are an average over the core, to ascertain the $N_e(r)$ and $T_e(r)$ one would need to measure the gradients.

Next, the reproducibility permits a detailed examination of Fig. 2, showing particularly disagreement at the Heβ line center between the observation and theoretical line shapes. The absence of an observed intensity dip at the line center may result from (1) opacity effects, (2) Li-like satellites, (3) spatial gradients in the target, or (4) ion dynamic effects [13]. First, we note that the optical depth of the 1–3 lines is low, consistent with the density measure, the core size measurement, and the relative emissivities of the 1–4 transitions, and does not affect the line profiles. Second, calculations including satellite lines show that at the measured values of N_e and T_e the higher-n satellites lines do not affect the line center emission. Third, we note that ion dynamics effects will fill in the dip at the line center and including these effects in the line-shape model improves the agreement with observation [13]. Ion dynamics indeed been have been confirmed at lower densities [14]; however, definitive experimental confirmation is still required at higher N_e. Although Haynes *et al.* [15] claimed to observe ion dynamic effects in laser-driven implosions, their analysis excluded spatial gradients, and the fact that effects of opacity were not treated rigorously compromised their conclusions.

To make a definitive test of ion dynamic effects, one can increase the mass of the fill gas ions (e.g., replacing D_2 with CD_4 or N_2) to slow the local electric-field fluctuations and recover the quasistatic limit for the inhomogeneous broadening of the Heβ line [13]. It is essential to keep the hydrodynamics of the target similar to the D_2 filled targets, to ensure that N_e and T_e peak near the same time to keep Heβ observable. Experiments replacing the D_2 fill gas with CD_4 and N_2 have shown that the central dip in the Ar XVII 1–3 line is *not* recovered.

Fourth, to see whether gradients can be the source of the filling of the dip, we resort to simulations. To study this we performed spectral simulations of the optically thin Heβ transition integrated over the spatial gradients *predicted* by the HYADES hydrodynamics simulations, but found that the N_e and T_e gradients are not severe enough to fill in the intensity dip at the Heβ line center. Thus we must assume that the details of the hydrodynamic simulations need to be verified, as this is the only facet of the analysis dependent on uncorroborated calculations.

In summary, we obtained the evolution of N_e and T_e during an indirectly driven implosion. In addition, we demon-

strated the reliability and reproducibility of implosion experiments. The experimental data provided confirmation of radiation-hydrodynamic simulations of an implosion, and, through the agreement of simulations with experiments, we inferred that N_e and T_e spatial gradients exist in the core. A discrepancy between experimental and theoretical Heβ line centers was observed, and several possible sources of the discrepancy were tested and found to be insufficient to explain the disagreement, including simulated N_e and T_e spatial gradients. Importantly, although ion dynamics effects on the line shapes potentially explain these differences, experiments showed that ion dynamic effects do *not* account for the discrepancy.

Finally, this work measured a simulation-free temporal history of an imploding core. This is critical to the understanding of three-dimensional spherically converging hydrodynamics, which in turn is central to the production of the hot dense matter for inertial fusion, and also provides a testbed for the study of radiative properties in extreme conditions.

[1] R. W. Lee, R. Petrasso, and R. W. Falcone, University of California Report No. UCRL119170 (Lawrence Livermore National Laboratory, 1995).

[2] B. A. Hammel, C. J. Keane, M. D. Cable, D. R. Kania, J. D. Kilkenny, R. W. Lee, and R. Pasha, Phys. Rev. Lett. **70**, 1263 (1993).

[3] B. A. Hammel, C. J. Keane, T. R. Dittrich, D. R. Kania, J. D. Kilkenny, R. W. Lee, and W. K. Levedahl, J. Quant. Spectrosc. Radiat. Transf. **51**, 113 (1994); N. Nishimura, T. Kiso, H. Shiraga, T. Endo, K. Fujita, A. Sunahara, H. Takabe, Y. Kato, and S. Nakai, Phys. Plasmas **2**, 2063 (1995).

[4] R. L. Kelly, J. Phys. Chem. Ref. Data **16**, (1987).

[5] C. J. Keane, B. A. Hammel, A. L. Osterheld, R. W. Lee, D. R. Kania, L. J. Suter, R. C. Mancini, C. F. Hooper, and N. D. Delamater, J. Quant. Spectrosc. Radiat. Transf. **51**, 147 (1994).

[6] A. Calisti, F. Khelfaoui, R. Stamm, B. Talin, and R. W. Lee, Phys. Rev. A **42**, 5433 (1990).

[7] J. K. Nash, J. M. Salter, W. G. Eme, and R. W. Lee, J. Quant. Spectrosc. Radiat. Transf. **54**, 283 (1995).

[8] E. M. Campbell, Laser Part. Beams **9**, 209 (1991).

[9] B. A. Hammel *et al.*, Rev. Sci. Instrum. **63**, 5083 (1992).

[10] P. M. Bell *et al.*, Rev. Sci. Instrum. **63**, 5072 (1992).

[11] M. D. Cable and S. P. Hatchett, J. Appl. Phys. **62**, 2233 (1987).

[12] J. T. Larsen and S. Lane, J. Quant. Spectrosc. Radiat. Transf. **51**, 179 (1994).

[13] N. C. Woolsey, A. Asfaw, B. A. Hammel, C. J. Keane, C. A. Back, A. Calisti, C. Mossé, R. Stamm, B. Talin, J. S. Wark, R. W. Lee, and L. Klein, Phys. Rev. E **53**, 6396 (1996).

[14] S. Glenzer *et al.*, J. Phys. B **27**, 5507 (1994).

[15] D. A. Haynes, Jr., D. T. Garber, C. F. Hooper, Jr., R. C. Mancini, Y. T. Lee, D. Bradley, J. Delettrez, R. Epstein, and P. A. Jaanimagi, Phys. Rev. E **53**, 1042 (1996).